



Research paper

Experimental study on the dynamic tensile mechanical properties of marble under water and oil conditions

Chaoxin Li¹, Dongyan Liu², Yunhui Zhu³

Abstract: To investigate the dynamic tensile properties and energy dissipation characteristics of marble in three different conditions: dry, water-saturated, and oil-saturated, a Brazilian disk splitting test was conducted using a 50 mm diameter Hopkinson pressure bar (SHPB) device. The findings indicate that the peak strain and dynamic tensile strength of the three conditions increase with strain rate, exhibiting a clear strain rate effect. Additionally, lubricating effects of water and oil weaken internal shear sliding friction, thus promoting crack expansion. Furthermore, immersion of fluid in marble weakens the cementation of internal mineral particles, leading to lower tensile strength of marble saturated with water and oil compared to dry marble under dynamic impact. When analyzing the energy dissipation of marble, both the absorption energy and dissipation energy density increase with oil strain rate, indicating a positive correlation. Moreover, numerical results obtained from ANSYS/LS-DYNA correspond well with experimental data, thus verifying and interpreting the experimental outcomes.

Keywords: dynamic splitting, split Hopkinson pressing bar (SHPB), energy dissipation, numerical simulation

¹MSc., College of Architecture and Engineering, Chongqing University of Science and Technology, Chongqing 401331, China, e-mail: 2021206112@cqust.edu.cn, ORCID: 0009-0000-5793-4291

²Prof., DSc., PhD., Eng., 1) Chongqing University, Chongqing 400000, China; 2) Chongqing College of Architecture and Technology, Chongqing 400000, China, e-mail: liudy@cqu.edu.cn

³MSc., College of Architecture and Engineering, Chongqing University of Science and Technology, Chongqing 401331, China, e-mail: 2021206110@cqust.edu.cn, ORCID: 0000-0001-9189-1870

1. Introduction

In recent years, with the rapid advancement of the social economy, the exploitation of mineral resources and infrastructure construction has expanded to underground areas. Traditional industries such as underground mining, water conservancy, construction, and oil and gas development have undergone further upgrades and transformations. In the exploitation of oil fields, the stress conditions of underground rocks are highly complex, often occurring in intricate seepage environments. The presence of water and oil in rocks has a profound impact on the stability of the rock mass, and can easily lead to rock mass instability or geological engineering disasters. Therefore, investigating the dynamic tensile mechanical properties of marble in different states holds significant importance in understanding the mechanical behavior of underground rocks and oilfield exploitation.

The investigation of dynamic tensile mechanical characteristics of rocks holds paramount importance. However, conducting direct dynamic tensile tests on rocks can be challenging. As a result, indirect experimental methods are commonly employed to measure the tensile properties of rocks. For instance, the Brazilian disk (BD) test, which was formally proposed by the International Society of Rock Mechanics (ISRM) in 1978 as a recommended method for determining the tensile properties of rock materials, has gained widespread recognition and application [1–3]. Notably, previous studies by Huang et al. [4,5] demonstrated that the dynamic tensile strength of Longyou sandstones exhibited a clear increase with higher loading rates under both dry and saturated conditions. Similarly, Zhou et al. [6,7] conducted a series of dynamic Brazilian cleavage tests on samples with varying moisture content and found that saturated specimens exhibited higher compressive strength compared to dry specimens at sufficiently high strain rates. Xi Daoying et al. [8] conducted uniaxial compression tests on dry and oil-saturated Dali rocks from Yunnan, and observed that both dry and oil-filled Dali rocks exhibited anisotropic behavior, with oil-saturated rocks showing stronger anisotropy and strain rate effects. Apart from investigating the tensile mechanical properties of rocks, there is a growing focus on studying rock mechanics problems [9] from the perspective of rock energy dissipation. The process of rock impact damage under dynamic loads often involves energy consumption and conversion [10]. G. Shuang and [11,12] conducted studies on energy dissipation laws during the dynamic fracture process of saturated coal samples through Brazilian splitting experiments. They compared incident energy, absorption energy, fracture energy, and residual kinetic energy of different impact velocities and stratified coal samples, and obtained the energy dissipation law during dynamic fracture processes of different stratified coal samples under impact loads.

Previous research has primarily focused on studying the dynamic mechanical characteristics and energy dissipation laws of rocks under dry and varying water content conditions. However, petroleum, being a fluid, can also have an impact on the mechanical properties of rocks. Hence, it is important to investigate the dynamic tensile mechanical properties of rocks under the condition of oil saturation. In this study, a combination of experimental tests and numerical simulations is used to investigate the dynamic tensile mechanical properties of marble in different fluid occurrences. The results will complement the understanding of the mechanical properties of marble under different fluid occurrences, and provide insights for stability analysis during oil exploitation activities.

2. Experimental methodology

2.1. Sample preparation

The rock materials used for the test were obtained from Leiyang, Hunan, to ensure consistency in physical and mechanical properties of the samples. Following the test requirements of the International Society of Rock Mechanics (ISRM) [13], cylindrical standard specimens with a diameter of 50 mm and a thickness of 25 mm were cut to eliminate the transverse inertia effect. The end faces of the specimens were carefully processed to ensure flatness and finish within 0.02 mm deviation. Initial screening was conducted based on the integrity and quality of the samples, and then the samples were further screened twice using a longitudinal wave velocity meter to select samples with similar longitudinal wave velocities for the test, as depicted in Figure 1. The selected samples were then subjected to different treatments, including drying, water saturation, and oil saturation. For the drying test, the samples were dried in a drying box at a temperature of 105°C for 24 hours. The fully water-saturated samples were prepared using a vacuum water saturation meter, and the samples were saturated with water for 48 hours before conducting the test. For the preparation of fully oil-saturated samples, dimethylsilicone oil (Table 1 for the parameters of dimethylsilicone oil) was used in this test. The samples were dried under vacuum at 105°C for 48 hours, and then saturated with oil to achieve an approximate full saturation condition [14].

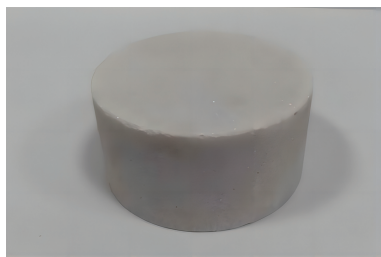


Fig. 1. Marble standard sample

Table 1. Dimethylsilicone oil parameters

Melting point (°C)	Boiling point (°C)	Density (g/mL)	Viscosity (mPa·s)
-59	150	0.764	100

2.2. Test equipment

The dynamic loading tests were performed by a modified SHPB system in set-up housed at the Central South University, China. The system mainly consists of an air gun, a cone-shaped striker, an incident bar (2.0 m in length), a transmitted bar (1.5 m in length),

an absorbing bar (0.8 m in length), an energy absorption device, a data acquisition device and strain gauges, as shown in Figure 2. The striker and all bars were made of high strength 40 Cr alloy steel, and the diameter, P-wave velocity, elastic modulus, yield strength, and density were 50 mm, 5410 m/s, 230 GPa, 800 MPa, and 7697 kg/m³, respectively.

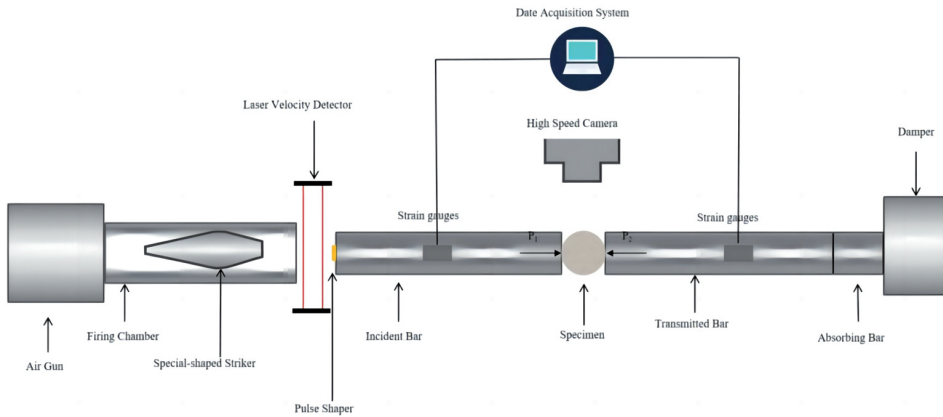


Fig. 2. Schematic diagram of the SHPB system

During the test, a pulse shaping technique was employed by placing a pulse shaper between the bullet and the incident bar to obtain a smooth waveform and reduce the amplitude of the oscillating waveform. The specimen was positioned between the incident bar and the transmission bar. To mitigate the inertial effects resulting from radial impact, petroleum jelly was applied as a lubricant on the contact surface between the specimen and the rods. Strain gauges were attached to both the incident and transmission rods, and the three waves were measured and recorded using a digital oscilloscope.

2.3. Verifying the stress equilibrium state

The bullet in the impact rod is subjected to air pressure, resulting in the generation of a one-dimensional stress wave that travels through the input rod and reaches the end of the input rod, transmitting the stress to the right. Through multiple transmissions and reflections, the stress at the two ends of the test specimen reaches a state of equilibrium. Figure 3a displays the electrical signals of the incident wave, reflection, and transmission wave of the sample, and a stress balance diagram of the sample under impact compression is obtained as shown in Figure 3b.

After 3–4 reflections [14], it can be observed from Figure 4 that the superimposed waveform of the transmission wave, incident wave, and reflection wave largely coincide, particularly the peak front curve, indicating that the sample reaches a state of stress balance during the loading process. The stress, strain, and strain rate of the sample can be obtained using the following formulas:

$$(2.1) \quad \sigma(t) = \frac{A_0 E}{2A} [\varepsilon_I(t) + \varepsilon_R(t) + \varepsilon_T(t)]$$

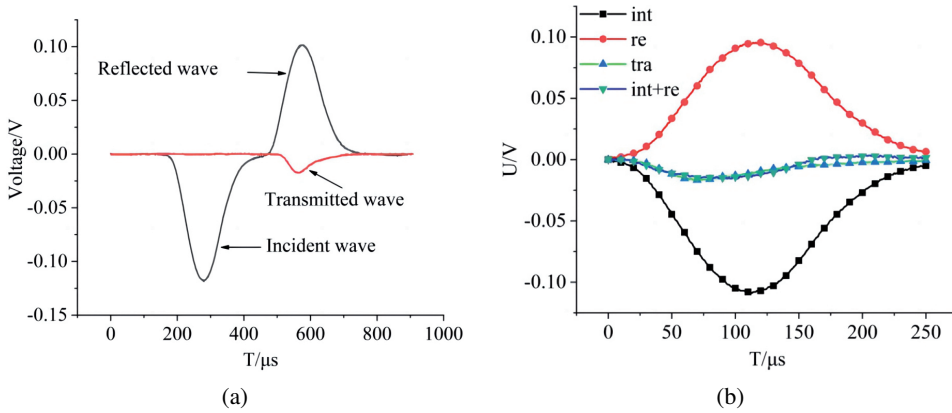


Fig. 3. (a) Electrical signals captured from the strain gauges; (b) Stress balance diagram of the test sample

$$(2.2) \quad \varepsilon(t) = \frac{C}{L} \int_0^T [\varepsilon_I(t) - \varepsilon_R(t) - \varepsilon_T(t)] dt$$

$$(2.3) \quad \dot{\varepsilon}(t) = -\frac{C}{L} \int_0^T [\varepsilon_I(t) - \varepsilon_R(t) - \varepsilon_T(t)]$$

where, $\sigma(t)$ – average axial stress, $\varepsilon(t)$ – average strain, $\dot{\varepsilon}(t)$ – average strain rate, ε_I – incident strain in compression bar, ε_R – reflected strain in compression bar, ε_T – transmitted strain in compression bar, E – elastic modulus of compression bar (GPa), A_0 – cross-sectional area of compression bar (m^2), C – wave velocity of compression bar, A – initial cross-sectional area of the specimen (m^2), L – initial length of the specimen (m).

3. Effect of strain rate on mechanical characteristics of marble under three conditions

The stress-strain curves of marble samples were obtained through dynamic splitting tests conducted at various strain rates under different states, including dry, water-saturated, and oil-saturated conditions. The dynamic mechanical parameters, such as peak stress and dynamic tensile strength, are summarized in Table 2 for comparison.

Figure 4 illustrates the variation of peak strain in marble specimens with respect to strain rate in dry, water-saturated, and oil-saturated conditions. It is evident from Figure 4 that as the strain rate increases, the peak strain at which marble specimens fail also increases, indicating a pronounced strain rate effect. Upon comparing the data, it is apparent that the peak strength of marble differs among the three states: dry > water-saturated > oil-saturated. In the water-saturated and oil-saturated states, the filling of water and oil in the

Table 2. Parameters of marbles under dynamic impact loading

Specimen No.	Condition	Strain rate (s ⁻¹)	Dynamic tensile strength (MPa)	Peak stress (10 ⁻³)
M-D-1	Dry	53.15	18.73	6.1
M-D-2		60.24	20.14	7.1
M-D-3		66.47	20.45	8.1
M-D-4		75.99	21.94	9.1
M-W-1	Water-Saturated	53.34	18.61	6.0
M-W-2		57.46	19.78	6.7
M-W-3		65.45	20.21	7.6
M-W-4		73.36	20.51	8.7
M-O-1	Oil-saturated	52.06	9.92	5.2
M-O-2		60.75	11.31	6.5
M-O-3		66.72	13.67	7.4
M-O-4		72.05	15.34	8.0

pores and cracks of marble weakens the inter-particle bonds, as the viscosity and fluidity of water and oil differ. The presence of liquid within the rock under external stress also induces pressure effects, thereby influencing the mechanical characteristics of marble. Hence, the peak strength is lower in water-saturated and oil-saturated states as compared to the dry state.

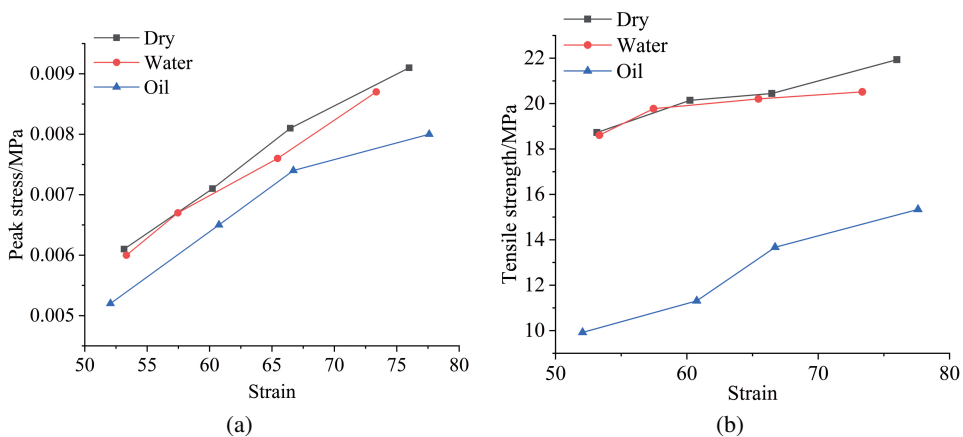


Fig. 4. (a) Relationship between peak strain and strain rate of dry and saturated rock samples; (b) Marble dynamic tensile strength and strain rate diagram

Figure 4b illustrates the variation of dynamic tensile strength of marble with respect to strain rate in different states, including dry, water-saturated and oil-saturated conditions. The combination of Table 2 and Figure 4b reveals that the dynamic tensile strength of marble exhibits a linear increase with strain rate in both dry, water-saturated and oil-saturated conditions. Among the three conditions, the dynamic tensile strength follows the order of dry > water-saturated > oil-saturated. This can be attributed to the weakening of internal mineral particles due to water saturation, which impacts the chemical reaction within the rock and ultimately leads to a degradation of tensile strength. In the case of oil-saturated marble, the presence of an oil film on the surface of the specimen enhances its lubricity, making it more susceptible to slip or shear under external forces, thus resulting in a reduction in dynamic tensile strength.

4. The mechanism of dynamic splitting energy dissipation in marble under three different states

The incident energy (W_I), reflection energy (W_R), transmission energy (W_T), and absorbed energy (W_S) of the specimen under SHPB dynamic compression can be calculated by Eq. (4.1–4.4) [15].

$$(4.1) \quad W_I = EC_0A_0 \int_0^t \varepsilon_I^2(t) dt$$

$$(4.2) \quad W_R = EC_0A_0 \int_0^t \varepsilon_R^2(t) dt$$

$$(4.3) \quad W_T = EC_0A_0 \int_0^t \varepsilon_T^2(t) dt$$

$$(4.4) \quad W_S = W_I - W_R - W_T$$

In the Split Hopkinson Pressure Bar (SHPB) test, the energy dissipation due to friction between the incident bar, the transmission bar, and the contact surface of the rock sample during the loading impact is often considered negligible. According to the law of conservation of energy, dissipation energy density (ω_d) and dissipation rate (φ) required for rock breaking can be calculated by Eqs. (4.5) and (4.6)

$$(4.5) \quad \omega_d = W_S/V$$

$$(4.6) \quad \varphi = W_S/W_I$$

Figure 5 depicts the exemplary energy-time curve of a dynamic tensile sample. As illustrated in Figure 5, diverse forms of energy exhibit an increase as time progresses, with negligible change in energy between 0 and 40 μ s. Subsequently, between 40 and 150, the

rate of energy growth accelerates, characterized by the steepest slope for incidence energy and the smallest slope for transmission energy. Once the time reaches 250 μs , the incidence loading is nearly complete, and the incident energy ceases to rise further. Considering the dynamic tensile stress-strain characteristics of the sample and the associated damage mode [16], the marble energy change curve can be discerned as comprising three distinct stages based on the absorption energy. The initial stage is the elastic deformation stage, wherein the absorbed energy is stored as elastic energy due to the closure of microcracks during compression of the rock sample. The subsequent stage is the rapid growth stage, marked by linear increase in incident energy, reflection energy, transmission energy, and absorption energy, with the absorbed energy being utilized to initiate and propagate cracks. The final stage is the plateau stage, wherein, after 150 μs , the incident energy, reflection energy, transmission energy, and absorption energy stabilize.

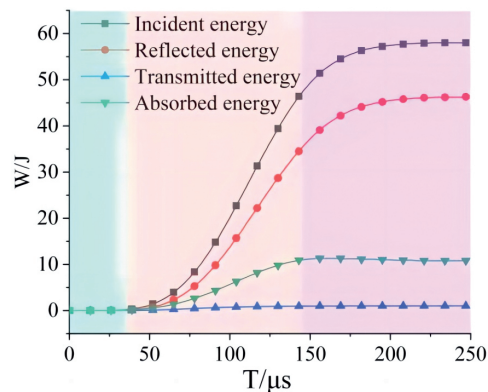


Fig. 5. Energy change curve of dry marble sample

In accordance with the principle of Split Hopkinson Pressure Bar (SHPB) test and the energy calculation formula, the energy values of marble samples during dynamic shock under dry and fully saturated water state were calculated, as presented in Table 3. To elucidate the energy distribution during marble tensile failure, the evolution characteristics of dissipation rate and energy density, which provide insights into the sample's capacity to absorb energy, were analyzed. Accordingly, the subsequent analysis focuses on the evolution patterns of marble dissipation rate and dissipation energy density in different conditions.

Energy dissipation is the underlying factor influencing the mechanical properties of rocks under varying strain rates [17]. Figure 6 presents the dynamic tensile strength and dissipation energy density of marble samples under different strain rates in dry, water-saturated, and oil-saturated states. From Figure 6, it can be observed that both dynamic tensile strength and dissipation energy density increase with higher strain rates, exhibiting a positive correlation. This indicates that as the strain rate increases, the deformation rate of the rock accelerates, leading to more activation of cracks within the rock mass. Consequently, the rock mass is capable of absorbing more energy, resulting in higher energy

Table 3. Energy data of marble samples under impact loading

Specimen No.	Condition	Strain rate (s ⁻¹)	Absorbed energy (J)	Energy dissipation density (J·mm ⁻³)
M-D-1	Dry	53.15	12.46	0.27
M-D-2		60.24	13.71	0.30
M-D-3		66.47	14.04	0.31
M-D-4		75.99	14.62	0.32
M-W-1	Water-Saturated	53.34	10.75	0.23
M-W-2		57.46	11.81	0.26
M-W-3		65.45	12.22	0.27
M-W-4		73.36	13.22	0.29
M-O-1	Oil-saturated	52.06	7.26	0.16
M-O-2		60.75	8.81	0.19
M-O-3		66.72	10.10	0.22
M-O-4		72.05	12.63	0.27

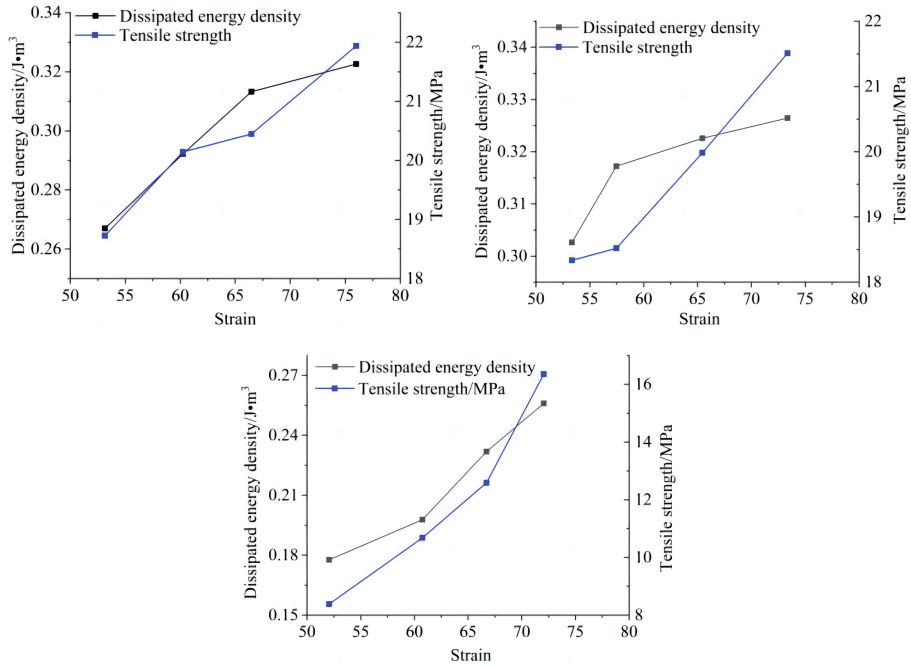


Fig. 6. Relationship between marble strain rate and dynamic tensile strength and energy dissipation density

dissipation per unit volume during deformation and failure. This enhances the dynamic tensile strength of marble to some extent, and also leads to increased fragmentation after failure.

5. Numerical simulation

The numerical simulation of the Split Hopkinson Pressure Bar (SHPB) dynamic impact was conducted using ANSYS software. The incident bar and transmission bar had lengths of 200 cm and 150 cm, respectively, with a diameter of 50 mm. The material model used for the incident and transmission bars was the native MAT_ELASTIC 001 model in LS-DYNA. In order to capture the fracture process of the sample, the RHT model in ANSYS/LS-DYNA was employed to describe the destructive behavior of the sample under impact load. Based on the basic physical parameters of marble, combined with the parameters in some concrete, and adjusted according to the results obtained by scholars [18–20], parameters of marble RHT model are finally determined as shown in Table 4. This constitutive model has been previously validated in the literature for studying the damage and fracture behavior of rock materials under dynamic load.

Table 4. The RHT model approximate parameters of the marble

Parameter symbol	Parameter value	Parameter symbol	Parameter value	Parameter symbol	Parameter value
ρ_0	2.8113E-6 kg/mm ³	f_c	0.1147 GPa	α_0	1.078
p_{el}	0.0287 GPa	β_c	0.0083	β_t	0.0115
A_1	0.3064 GPa	A_2	0.5147 GPa	A_3	0.3146 GPa
B_0	1.68	B_1	1.68	T_1	15.84
T_2	0 GPa	G	10.5 GPa	$\dot{\epsilon}^c$	3.0E19 m·s ⁻¹
$\dot{\epsilon}_0^c$	3.0E-11 m·s ⁻¹	$\dot{\epsilon}_0^t$	3.0E-12 m·s ⁻¹	f_s^*	0.38
$\dot{\epsilon}^t$	3.0E19 m·s ⁻¹	D_2	1.0	g_c^*	0.53
B	0.0105	g_t^*	0.7	ϵ_p^m	0.01
A	1.6	n	0.61	p_{comp}	0.06
f_t^*	0.08	Q_0	0.6805	N	3.0
ξ	0.5	D_1	0.04	n_f	0.61
A_f	1.6	P_{crush}	39		

Figure 7 presents the overall model diagram of the simulated SHPB splitting test, with the transmission bars and incident bars depicted on the left and right sides, respectively, designated as PART 1, and the sample in the middle designated as PART 2.

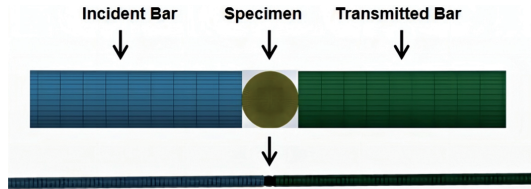


Fig. 7. Numerical simulation model of SHPB

In the numerical simulation of Split Hopkinson Pressure Bar (SHPB), the incident signal is used to simulate the impact of the bullet. As the stress waveform generated by the bullet striking the incident rod is a semi-sine wave, the incident wave in the simulation is approximated to a sine function and applied to the end of the incident rod. The mathematical form of the function is as follows:

$$(5.1) \quad \sigma_I = \frac{1}{2}A \left(1 - \cos \frac{2\pi}{T}t \right) \quad (0 < t < T)$$

where, T – total duration of the incident waveform, A – peak strain of the incident wave.

From Figure 8, it is evident that the stress-strain curves of marble in oil-saturated and water-saturated states exhibit a significant level of conformity with the stress-strain curves

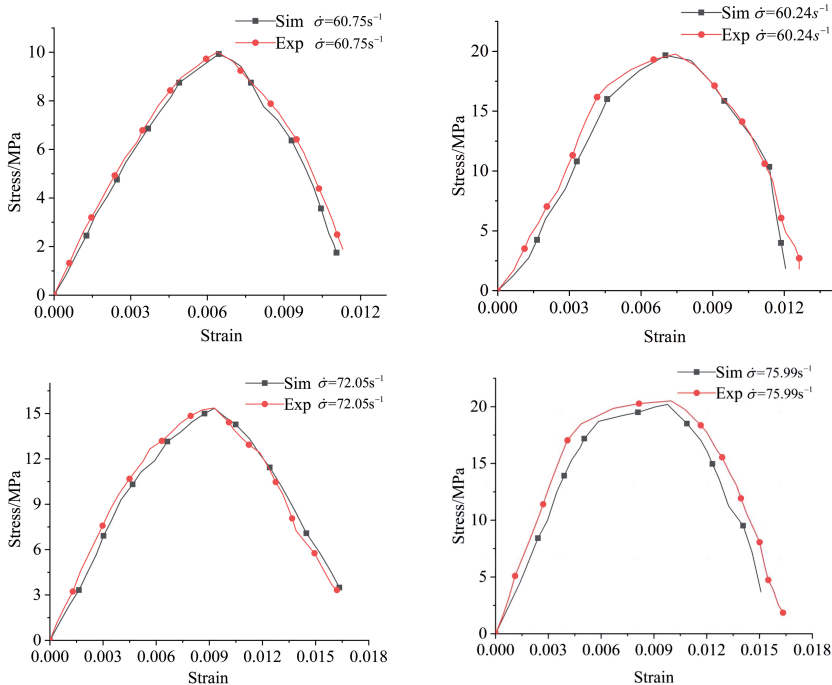


Fig. 8. Stress-strain curves of marble under different strain rates

obtained from numerical simulations at varying strain rates. The ascending segments of the stress curves show a close alignment, with minor variations in peak stress values.

To validate the efficacy of the simulation, Figure 9 presents a comparative analysis of marble samples subjected to numerical simulation and experimental tests in oil-saturated state at varying strain rates. As depicted in the figure, the damage patterns of samples exhibit differences at different strain rates. In general, as the strain rate increases, the degree of sample crushing gradually intensifies. Initially, at the unbroken impact pressure, the sample remains intact, but as the impact pressure reaches the critical point, the sample experiences damage and fragmentation, eventually resulting in several large rock blocks and numerous powder cuttings. This indicates that the degree of sample crushing becomes more severe with higher strain rates. Furthermore, at different strain rates, the marble sample makes contact with the rod end and primarily exhibits tensile damage along the loading direction. The stress at the contact position between the sample and the pressing rod increases with higher strain rates, leading to an increase in small volume fragments after sample damage, indicative of more severe damage.





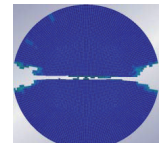
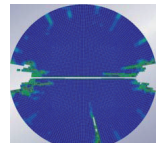
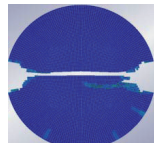
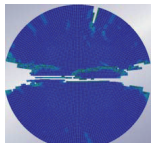
Strain rate	$\dot{\sigma} = 52.06 \text{ s}^{-1}$	$\dot{\sigma} = 60.75 \text{ s}^{-1}$	$\dot{\sigma} = 66.72 \text{ s}^{-1}$	$\dot{\sigma} = 72.05 \text{ s}^{-1}$
Experiment				
Simulation				

Fig. 9. Comparison of numerical simulation and test results

6. Conclusions

Based on the findings from dynamic splitting tests conducted on marble in dry, water-saturated, and oil-saturated states, a comprehensive analysis of the strain rate effect was carried out, focusing on the dynamic mechanical characteristics and energy dissipation. The main conclusions were as follows:

1. Through the analysis of strain rate effects on marble under different conditions (dry, oil-saturated and water-saturated), it was observed that the peak strain of the rock increases with higher strain rates. The order of peak strain magnitude for different states is as follows: dry > water-saturated > oil-saturated. The dynamic tensile strength also follows the same order: dry > water-saturated > oil-saturated.
2. During the early stages of the dynamic splitting tensile experiments, both the reflection energy and absorption energy of the marble specimens increase linearly with the incident energy. The order of absorption energy for different states is as follows:

dry > water-saturated > oil-saturated, indicating that the rock sample consumes more energy in a dry state. Both dynamic tensile strength and dissipation energy density show a positive correlation with strain rate, increasing as the strain rate increases.

3. Finite element numerical simulations using ANSYS/LS-DYNA software were conducted in this chapter, and the simulated stress-strain curves at different strain rates were found to be in good agreement with the experimental curves. The macroscopic damage modes of the sample loading process were analyzed through numerical simulation, and the simulation results were consistent with the experimental results.

References

- [1] ISRM Testing Commission, "Suggested method for determining tensile strength of rock materials", *International Journal of Rock Mechanics and Mining Sciences & Geomechanics Abstracts*, vol. 15, no. 3, pp. 99–103, 1978.
- [2] A.R. Torabi, A. Campagnolo, and F. Berto, "Local strain energy density to predict mode II brittle fracture in Brazilian disk samples weakened by V-notches with end holes", *Materials & Design*, vol. 69, pp. 22–29, 2015, doi: [10.1016/j.matdes.2014.12.037](https://doi.org/10.1016/j.matdes.2014.12.037).
- [3] F. Berto and M.R. Ayatollahi, "Fracture assessment of Brazilian disc samples weakened by blunt V-notches under mixed mode loading by means of local energy", *Materials & Design*, vol. 32, no. 5, pp. 2858–2869, 2011, doi: [10.1016/j.matdes.2010.12.034](https://doi.org/10.1016/j.matdes.2010.12.034).
- [4] S. Huang, R. Chen, and K.W. Xia, "Quantification of dynamic tensile parameters of rocks using a modified Kolsky tension bar apparatus", *Journal of Rock Mechanics and Geotechnical Engineering*, vol. 2, no. 2, pp. 162–168, 2010, doi: [10.3724/SP.J.1235.2010.00162](https://doi.org/10.3724/SP.J.1235.2010.00162).
- [5] S. Huang, F. Yan, K.W. Xia, et al., "An experimental study of the rate dependence of tensile strength softening of Longyou sandstone", *Rock Mechanics and Rock Engineering*, vol. 43, pp. 677–683, 2010, doi: [10.1007/s00603-010-0083-8](https://doi.org/10.1007/s00603-010-0083-8).
- [6] Z.L. Zhou, X. Cai, Y. Zhao, et al., "Strength characteristics of dry and saturated rock at different strain rates", *Transactions of Nonferrous Metals Society of China*, vol. 26, no. 7, pp. 1919–1925, 2016, doi: [10.1016/S1003-6326\(16\)64314-5](https://doi.org/10.1016/S1003-6326(16)64314-5).
- [7] Z.L. Zhou, X. Cai, Y. Zhao, et al., "Influence of water content on mechanical properties of rock in both saturation and drying processes", *Rock Mechanics and Rock Engineering*, vol. 49, no. 8, pp. 3009–3025, 2016, doi: [10.1007/s00603-016-0987-z](https://doi.org/10.1007/s00603-016-0987-z).
- [8] D.Y. Xi, B. Liu, S.Y. Bai, et al., "Anisotropy and strain rate effects of saturated rocks", presented at Chinese Geophysical Society, 21–24 October 2000, Wuhan, China, 2000.
- [9] F.Q. Gong, P.L. Zhang, and L. Xu, "Damage constitutive model of brittle rock under uniaxial compression based on linear energy dissipation law", *International Journal of Rock Mechanics and Mining Sciences*, vol. 160, 2022, doi: [10.1016/j.ijrmms.2022.105273](https://doi.org/10.1016/j.ijrmms.2022.105273).
- [10] Y. Deng, M. Chen, et al., "Theoretical analysis and experimental research on the energy dissipation of rock crushing based on fractal theory", *Journal of Natural Gas Science and Engineering*, vol. 33, pp. 231–239, 2016, doi: [10.1016/j.jngse.2016.05.020](https://doi.org/10.1016/j.jngse.2016.05.020).
- [11] S. Gong, L. Zhou, et al., "Investigation of dynamic fracture behavior and energy dissipation of water-bearing coal under impact load", *Engineering Fracture Mechanics*, vol. 275, 2022, doi: [10.1016/j.engfracmech.2022.108793](https://doi.org/10.1016/j.engfracmech.2022.108793).
- [12] S. Gong and Y.X. Zhao, "Experimental study on the influence of bedding on dynamic fracture and energy dissipation of coal rock", *The Journal of Rock Mechanics and Engineering*, vol. 36, no. S2, pp. 3723–3731, 2017, doi: [10.13722/j.cnki.jrme.2017.0630](https://doi.org/10.13722/j.cnki.jrme.2017.0630).
- [13] Z.L. Wang, H.C. Wang, J.G. Wang, et al., "Finite element analyses of constitutive models performance in the simulation of blast-induced rock cracks", *Computers and Geotechnics*, vol. 135, 2021, doi: [10.1016/j.compgeo.2021.104172](https://doi.org/10.1016/j.compgeo.2021.104172).

- [14] H. Cao and X.Y. Zhang, “Study on uniaxial impact compression characteristics of basalt fiber cement soil”, *Archives of Civil Engineering*, vol. 68, no. 1, pp. 667–668, 2022, doi: [10.24425/ace.2022.140193](https://doi.org/10.24425/ace.2022.140193).
- [15] X. B. Li and F.Q. Gong, “Reference method for determining the sample size in the rock SHPB test”, *Journal of Vibration and Shock*, vol. 32, no.17, pp. 24–28, 2013, doi: [10.13465/j.cnki.jvs.2013.17.005](https://doi.org/10.13465/j.cnki.jvs.2013.17.005).
- [16] F.J. Xie, J.S. Zhang, and J.H. Chen, “Dynamic damage model of rock under impact loads of compression and tension”, *Journal of Central South University (Science and Technology)*, vol. 50, no. 2, pp. 420–427, 2019 [in Chinese].
- [17] J. Zhu, J.H. Deng, Y.J. Ma, et al., “Experimental study on the competing effects of strain rate and water weakening on compressive strength of saturated rocks”, *Engineering Geology*, vol. 310, 2022, doi: [10.1016/j.enggeo.2022.106873](https://doi.org/10.1016/j.enggeo.2022.106873).
- [18] C.Z. Wang, A.J. Chen, Z.Q. Li, et al., “Experimental and numerical investigation on penetration of clay masonry by small high-speed projectile”, *Defence Technology*, vol. 17, no. 4, pp. 1514–1530, 2021, doi: [10.1016/j.dt.2020.09.017](https://doi.org/10.1016/j.dt.2020.09.017).
- [19] H.C. Li, D.S. Liu, L. Zhao, et al., “Study on parameters determination of Marble RHT Model”, *Transactions of Beijing Institute of Technology*, vol. 37, no. 8, pp. 801–806, 2017, doi: [10.15918/j.tbit1001-0645.2017.08.006](https://doi.org/10.15918/j.tbit1001-0645.2017.08.006).
- [20] C. Reifarth, R. Castedo, A.P. Santos, et al., “Numerical and experimental study of externally reinforced RC slabs using FRPs subjected to close-in blast loads”, *International Journal of Impact Engineering*, vol. 156, 2021, doi: [10.1016/j.ijimpeng.2021.103939](https://doi.org/10.1016/j.ijimpeng.2021.103939).

Received: 2023-04-21, Revised: 2023-06-20